

Electronic Supplementary Information

**Multi-color tunable circularly polarized luminescence in one
single AIE system**

Hongxing Shang^{a}, Zeyang Ding^{a*}, Yue Shen^a, Bing Yang^a, Minghua Liu^{b*} and Shimei Jiang^{a*}*

^aState Key Laboratory of Supramolecular Structure and Materials. College of Chemistry, Jilin University. Changchun, 130012, P. R. China.

E-mail: smjiang@jlu.edu.cn

^bCAS Key Laboratory of Colloid, Interface and Thermodynamics, Institute of chemistry, Chinese Academy of Sciences. Beijing, 100190, P. R. China.

E-mail: liumh@iccas.ac.cn

**These authors contributed equally to this work.*

Materials and Methods

^1H NMR spectra were recorded on a Bruker AVANCE 500 MHz spectrometer (tetramethylsilane as the internal standard). ^{13}C NMR spectra were recorded on a Bruker AVANCE 125 MHz spectrometer. Mass spectra were performed on an Autoflex speed TOF/TOF mass spectrometer. Element analyses (C, H and N) were determined using a Perkin-Elmer 2400 elemental analyzer. Scanning electron microscopy (SEM) images were obtained from a JEOL JEM-6700F at 3 kV, with the samples sputtered with a layer of platinum (ca. 2 nm thick) prior to imaging to improve conductivity. Powder X-ray diffraction (XRD) patterns were generated by using a Rigaku D/MAX 2500/PC X-ray diffractometer with CuK α radiation ($\lambda = 0.15418$ nm). Differential scanning calorimetry (DSC) measurements were performed on a Netzsch DSC 204 using a. at a 10 °C/min scanning rate under nitrogen. Thermal gravimetric analyzer (TGA) measurements were performed on a TA Q500 using a. at a 10 °C/min scanning rate under nitrogen. The rheological properties were studied on a TA instrument (AR2000 Rheometer) equipped with an aluminium plate of 25 mm diameter. The samples were sandwiched between the two plates with a gap of 0.5 mm throughout the experiments. Circular dichroism (CD) spectra were carried out on a Bio-Logic MOS-450 spectropolarimeter with a step size of 0.5 nm and speed of 4 nm s $^{-1}$ at 25 °C. UV-vis absorption spectra were taken on a Shimadzu 3100 UV-VIS-NIR recording spectrophotometer. The fluorescence spectra were scanned with a Shimadzu RF-5301PC spectrophotometer. The CPL was measured using a JASCO CPL-200 spectrometer, and the value of g_{lum} is defined as $g_{\text{lum}} = 2 \times [\text{ellipticity}/(32980/\ln 10)]/\text{total fluorescence intensity at the CPL extremum}$. Fluorescence lifetime and quantum efficiency were carried out with Edinburgh fluorescence spectrometer (FLS980) with an integrating sphere. The ground-state geometries were optimized under the B3LYP/6-31G (d, p) level, which was well known to provide molecular geometries in good agreement with the experiment. The excited-state geometry was optimized by time-dependent density functional theory (TD-DFT) with the B3LYP functional at the same basis set level. The emission properties were obtained using TD-m062x/6-31G (d, p) at the excited state geometries. The solvent effect in DMF were mimicked by using the polarizable continuum model (PCM). In order to examine the character of excited-states, natural transition orbitals (NTOs) were evaluated for the lowest singlet excited-states.

Synthesis and Characterization of Compounds

4-(pyridin-4-yl)benzaldehyde (**1**) and *2-(4'-hydroxybiphenyl-4-yl)acetonitrile* (**2**) were previously reported in the literature by using Suzuki coupling reaction, respectively.^{1, 2}

4-(pyridin-4-yl)benzaldehyde (**1**): A mixture of 4-bromopyridine hydrochloride (1.50 g, 7.71 mmol), K $_2$ CO $_3$ (4.26 g, 30.9 mmol), 4-formylphenylboronic acid (1.50 g, 10.00 mmol) and tetrakis(triphenylphosphine)palladium(0) (0.10 g, 0.88 mmol) in dioxane (30 mL) and water (7.5 mL) was refluxed for 12 h. After cooling to room temperature water was added and the mixture was extracted with dichloromethane. The combined organic layers were dried with magnesium sulfate, filtered and concentrated and the residue was purified by chromatography on silica gel (hexanes/ethyl acetate = 1:2) to give 1.30 g of product as a slightly yellow solid (yield = 92%). ^1H NMR (500 MHz, CDCl $_3$) δ 10.10 (s, 1H), 8.73 (dd, $J = 4.6, 1.5$ Hz, 2H), 8.02 (d, $J = 8.3$ Hz, 2H), 7.81 (d, $J = 8.2$ Hz, 2H), 7.55 (dd, $J = 4.5, 1.6$ Hz, 2H).

2-(4'-hydroxybiphenyl-4-yl)acetonitrile (2): (4-Bromo-phenyl)-acetonitrile (2.1 g, 10.71 mmol), 4-hydroxybenzeneboronic acid (1.5 g, 10.88 mmol), and tetrakis(triphenylphosphine)palladium(0) (0.10 g, 0.88 mmol) were dissolved in 60 mL of THF and 30 mL of 2 N sodium carbonate aqueous solution and reacted for 12 h at 77 °C. The reaction mixture was then poured into brine solution, extracted with ethyl acetate, and dried over anhydrous magnesium sulfate. Finally, the solvent was removed under reduced pressure. The crude reaction mixture was purified by column chromatography (silica gel, ethyl acetate/n-hexane: 1/1) to give 1.50 g of product as a white solid (yield =71%). ¹H NMR (500 MHz, CDCl₃) δ 7.55 (d, *J* = 8.1 Hz, 2H), 7.47 (d, *J* = 8.6 Hz, 2H), 7.38 (d, *J* = 8.0 Hz, 2H), 6.92 (d, *J* = 8.6 Hz, 2H), 4.80 (s, 1H), 3.79 (s, 2H).

(Z)-2-(4'-hydroxybiphenyl-4-yl)-3-(4-(pyridin-4-yl)phenyl)acrylonitrile (3): Compound **1** (0.915 g, 5 mmol) and compound **2** (1.045 g, 5 mmol) were added to a clear solution of sodium (0.058 g, 25 mmol) in methanol (20 mL), and the reaction mixture was stirred for about 24 h at room temperature until an orange precipitates were formed. Then, the precipitates were filtered and washed with methanol and water three times to obtain an orange powder (1.50 g, 80%). ¹H NMR (500 MHz, DMSO) δ 10.10 (s, 1H), 8.70 (dd, *J* = 10.8, 5.8 Hz, 2H), 8.16 – 8.08 (m, 2H), 8.06 (s, 1H), 8.02 (d, *J* = 8.3 Hz, 2H), 7.81 (dd, *J* = 13.5, 7.4 Hz, 2H), 7.72 (d, *J* = 8.4 Hz, 2H), 7.57 (d, *J* = 8.1 Hz, 2H), 7.48 (d, *J* = 8.6 Hz, 2H), 7.40 (d, *J* = 8.5 Hz, 2H), 7.34 (d, *J* = 8.1 Hz, 2H), 6.72 (dd, *J* = 14.8, 8.5 Hz, 2H).

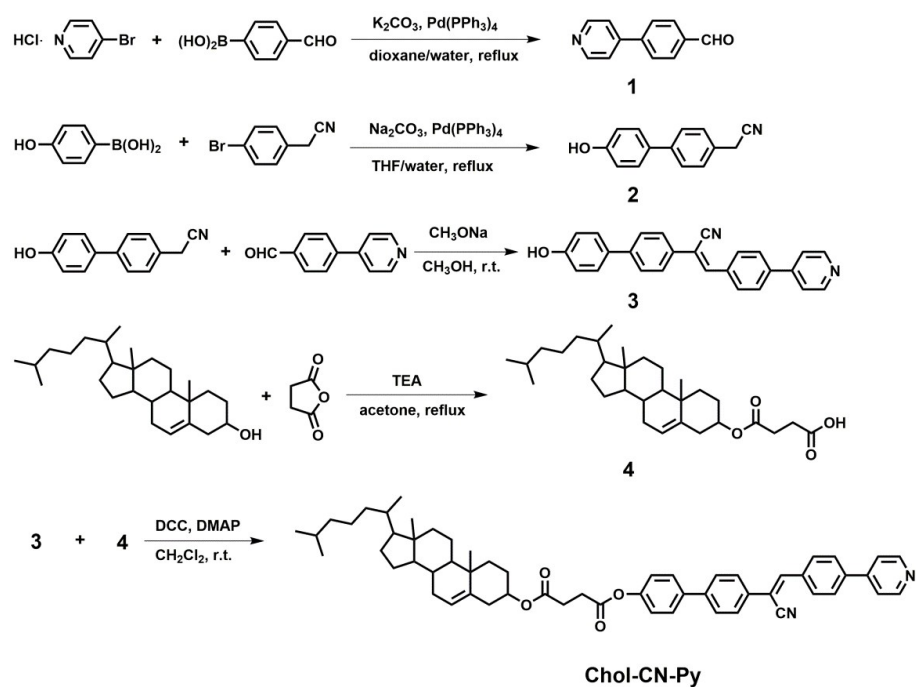
Compound **4** was previously reported in the literature.³

Chol-CN-Py: 1,3-dicyclohexylcarbodiimide (DCC) (0.48 g, 2.2 mmol) and 4-dimethylaminopyridine (DMAP) (0.06 g, 0.5 mmol) were added into compound **4** (1.17 g, 2.2 mmol) and Compound **3** (0.75 g, 2 mmol) in dried dichloromethane (50 mL) after cooling from ice bath. The reaction mixture was stirred for 4 days at room temperature. Then filtered to remove the insoluble substance, and the solvent was evaporated by reduced pressure. The powder was washed with ethyl acetate and ethanol in sequence. A light yellow powder was obtained (0.75 g, 45%). ¹H NMR (500 MHz, CDCl₃) δ 8.72 (d, *J* = 5.3 Hz, 2H), 8.04 (d, *J* = 8.3 Hz, 2H), 7.78 (dd, *J* = 8.0, 6.0 Hz, 4H), 7.67 (d, *J* = 8.3 Hz, 2H), 7.64 (s, 1H), 7.63 (d, *J* = 5.9 Hz, 2H), 7.57 (d, *J* = 5.7 Hz, 2H), 7.21 (d, *J* = 8.5 Hz, 2H), 5.38 (s, 1H), 4.66 (m, 1H), 2.92 (t, *J* = 6.6 Hz, 2H), 2.75 (t, *J* = 6.6 Hz, 2H), 2.35 (m, 2H), 2.01 (d, *J* = 12.6 Hz, 2H), 1.87 (m, 3H), 1.73 – 0.75 (m, 36H), 0.68 (s, 3H). ¹³C NMR (125 MHz, CDCl₃): δ = 171.47, 171.05, 150.59, 150.02, 147.59, 141.49, 140.64, 139.73, 139.54, 137.63, 134.60, 133.18, 130.09, 128.12, 127.73, 127.59, 126.53, 122.81, 122.07, 117.80, 112.29, 74.62, 56.70, 56.15, 50.03, 42.32, 39.73, 39.52, 38.10, 36.97, 36.61, 36.19, 35.80, 31.92, 31.87, 29.49, 28.24, 28.02, 27.78, 24.29, 23.84, 22.83, 22.57, 21.04, 19.33, 18.73, 11.87. MALDI-TOF (*m/z* (%)) calcd: 843.14; Found: 843.54. Anal. calcd for C₅₇H₅₅N₂O₄: C 81.20; H 7.89; N 3.32; O 7.59. Found: C 80.10; H 7.98; N 3.23; O 8.69.

1 D. Trawny, L. Vandromme, J. P. Rabe and H.- U. Reissig, *Eur. J. Org. Chem.*, 2014, 4985-4992.

2 H. Nam, B. Boury and S. Y. Park, *Chem. Mater.*, 2006, **18**, 5716-5721.

3 P. Xue, R. Lu, G. Chen, Y. Zhang, H. Nomoto, M. Takafuji and H. Ihara, *Chem. Eur. J.*, 2007, **13**, 8231-8239.



Scheme S1. Synthesis procedure of **Chol-CN-Py**.

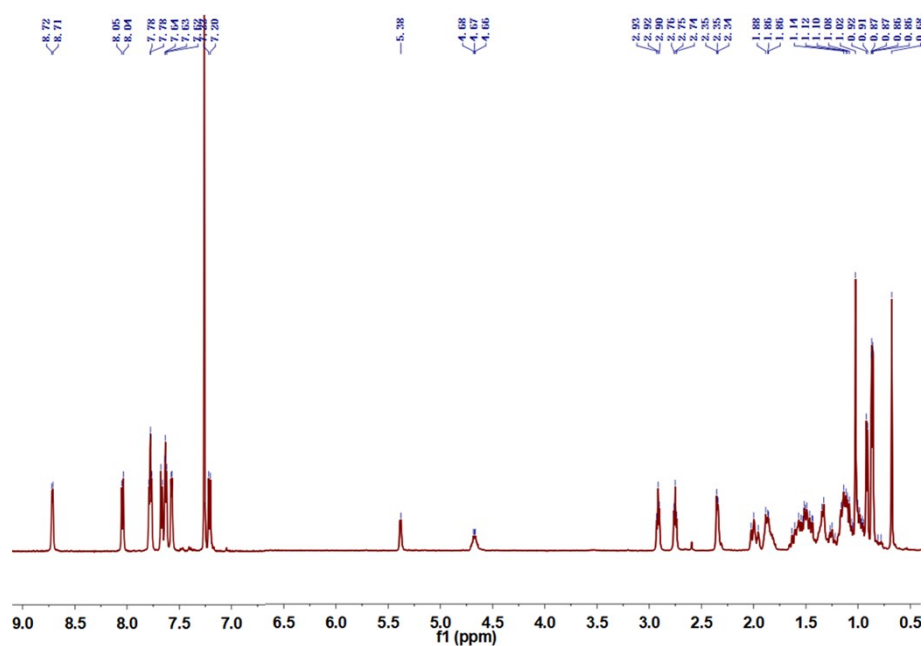


Fig. S1 ¹H NMR (500 MHz) spectrum of **Chol-CN-Py** in CDCl₃.

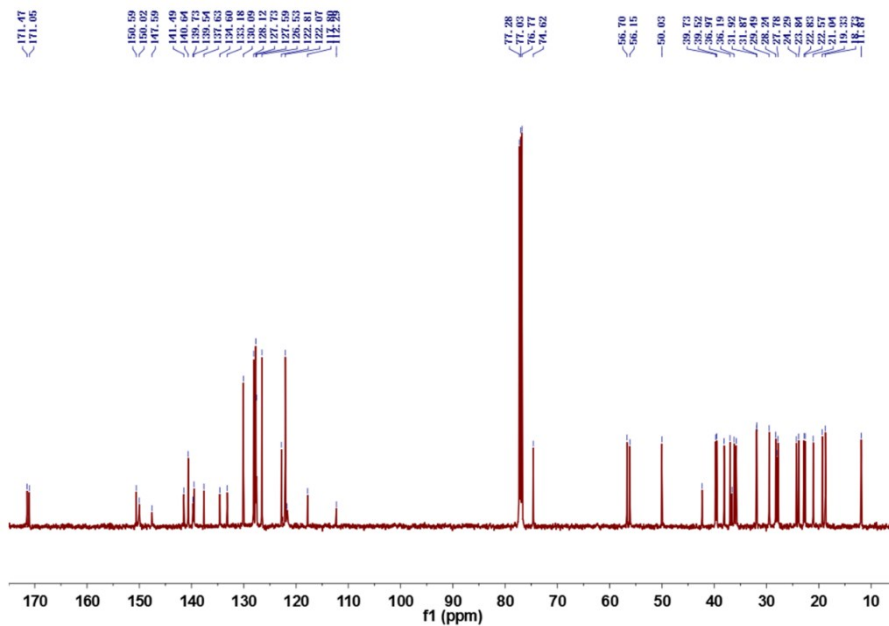


Fig. S2 ^{13}C NMR (125 MHz) spectrum of Chol-CN-Py in CDCl_3 .

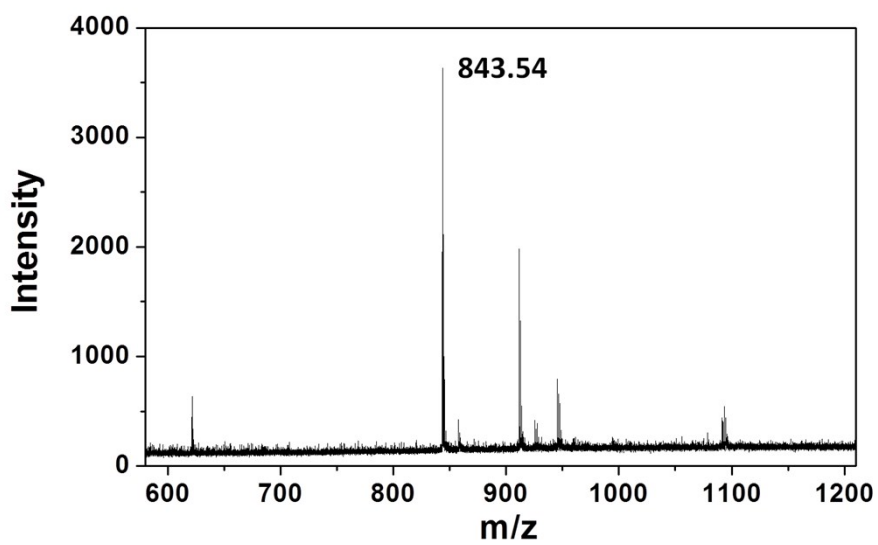


Fig. S3 MALDI-TOF spectrum of Chol-CN-Py.

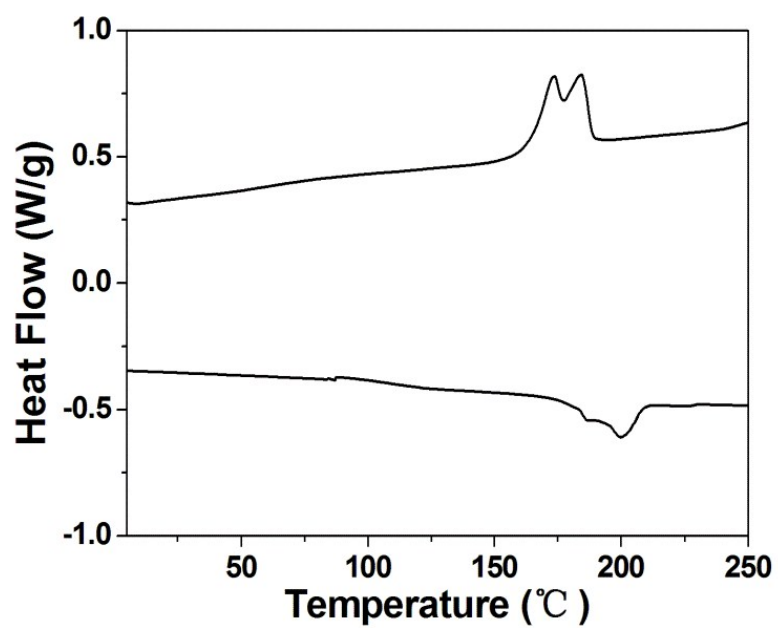


Fig. S4 DSC curves of Chol-CN-Py.

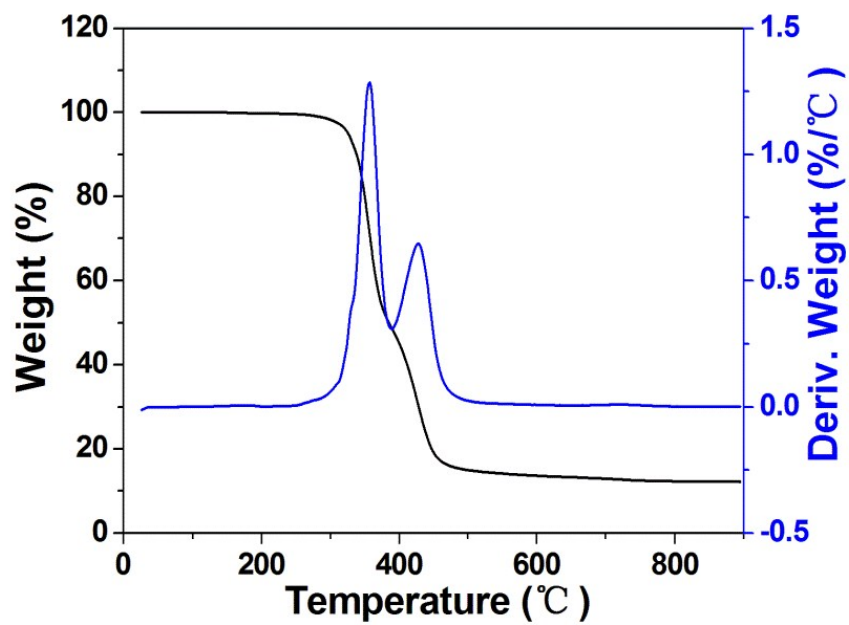


Fig. S5 TGA curves of Chol-CN-Py.

Table S1. Gelation properties of **Chol-CN-Py** in various solvents.

Solvent	Phase	Solvent	Phase
DMSO	G (10)	Dichloromethane	S
DMF	P	Ethanol	I
Acetone	P	Methanol	I
Ethyl acetate	P	Cyclohexane	I
THF	S	n-Hexane	I
Dichloroethane	S	p-Xylene	P
Chloroform	S	Toluene	P

G, gel; I, insoluble; P, precipitation; S, solution. Numbers in parentheses indicate the critical gelator concentration (CGC, mg/mL).

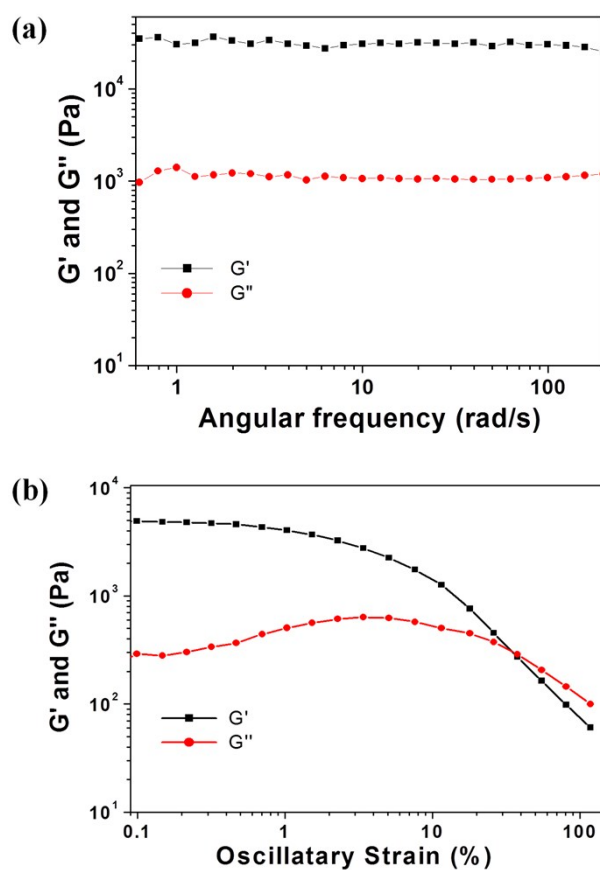


Fig. S6 (a) Evolution of G' and G'' as functions of angular frequency for gel. (b) Amplitude dependencies of G' and G'' of gel as functions of the shear strain. The frequency is 1 Hz.

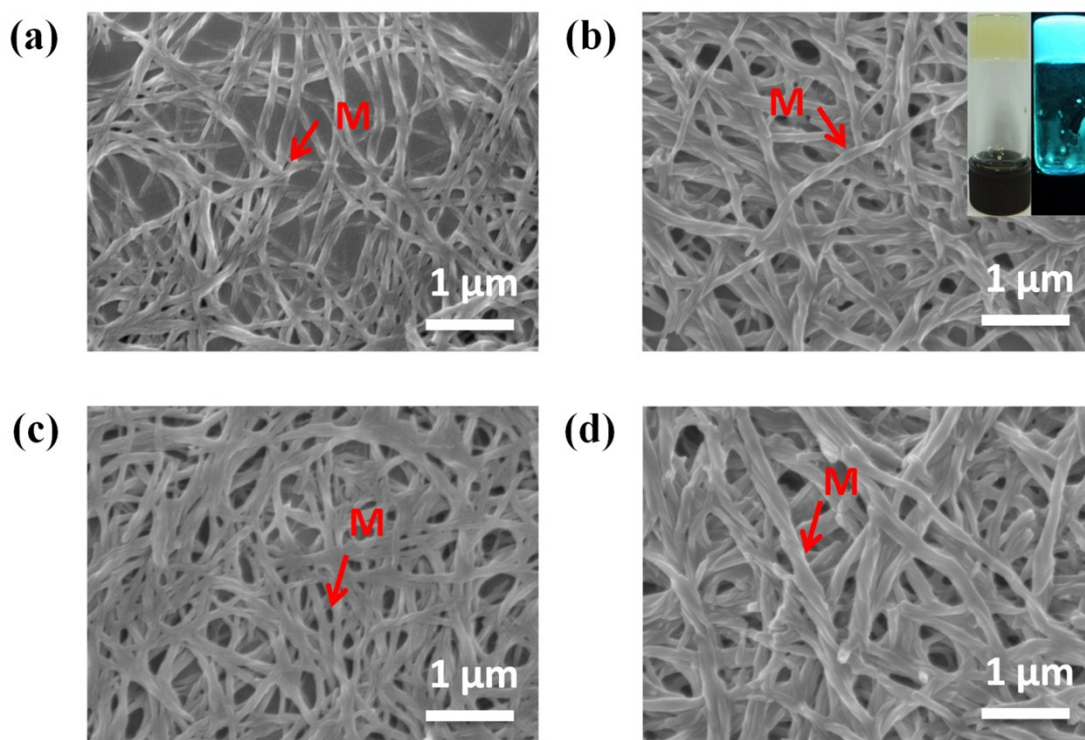


Fig. S7 SEM images of **Chol-CN-Py** self-assembled structure in different concentrations ((a) 8, (b) 10, (c) 15, (d) 20 mg/mL), indicating the same helix direction. Insets of (b): photographs of the corresponding gels under ambient light (left) and illumination at 365 nm (right).

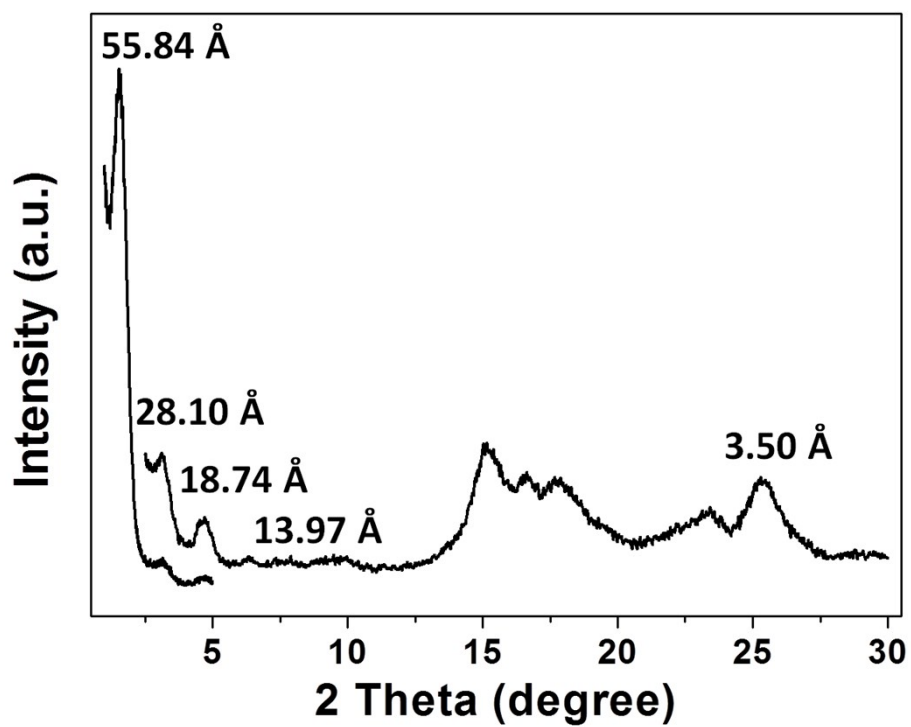


Fig. S8 X-ray diffraction patterns of **Chol-CN-Py** xerogel.

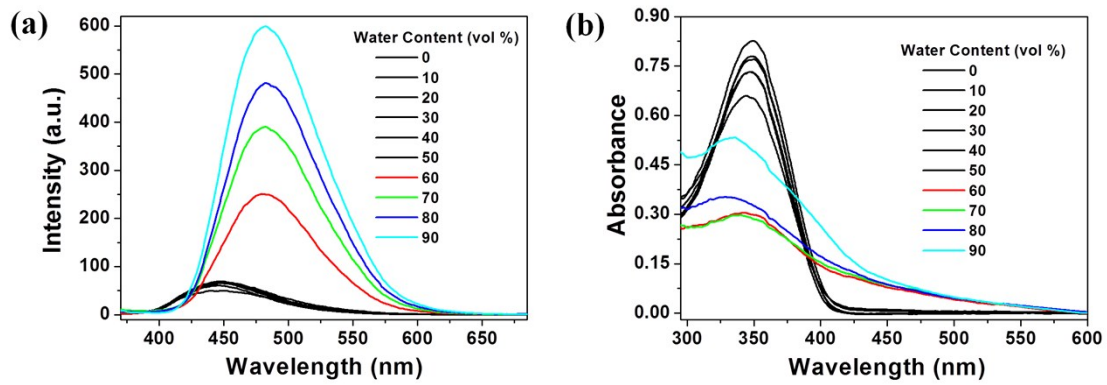


Fig. S9 (a) Fluorescence ($\lambda_{\text{ex}} = 350 \text{ nm}$) and (b) UV-vis absorption spectra of **Chol-CN-Py** (10^{-5} M) in THF/water mixtures with different water contents (from 0% to 90%).

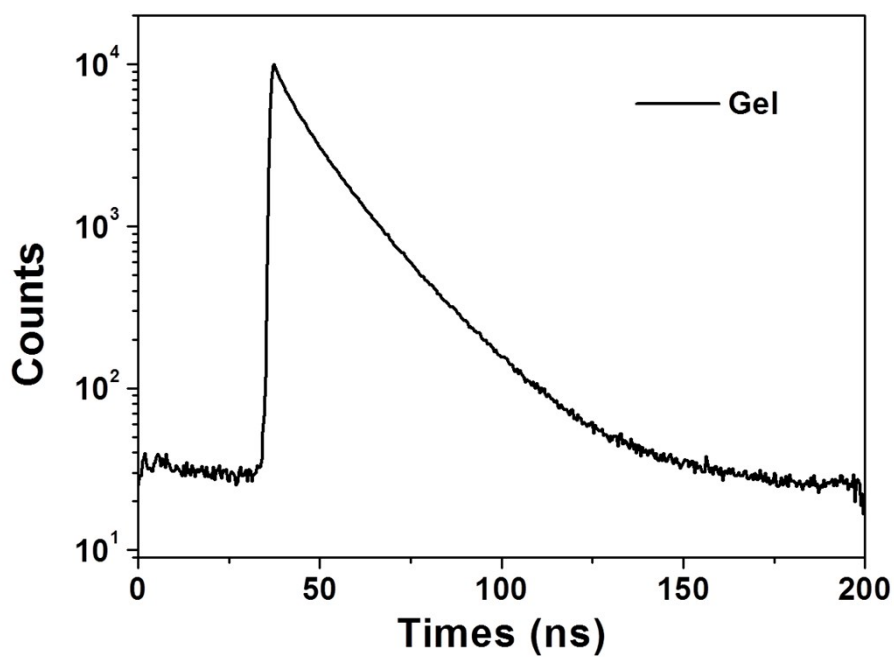


Fig. S10 Fluorescence kinetic profiles of **Chol-CN-Py** gel.

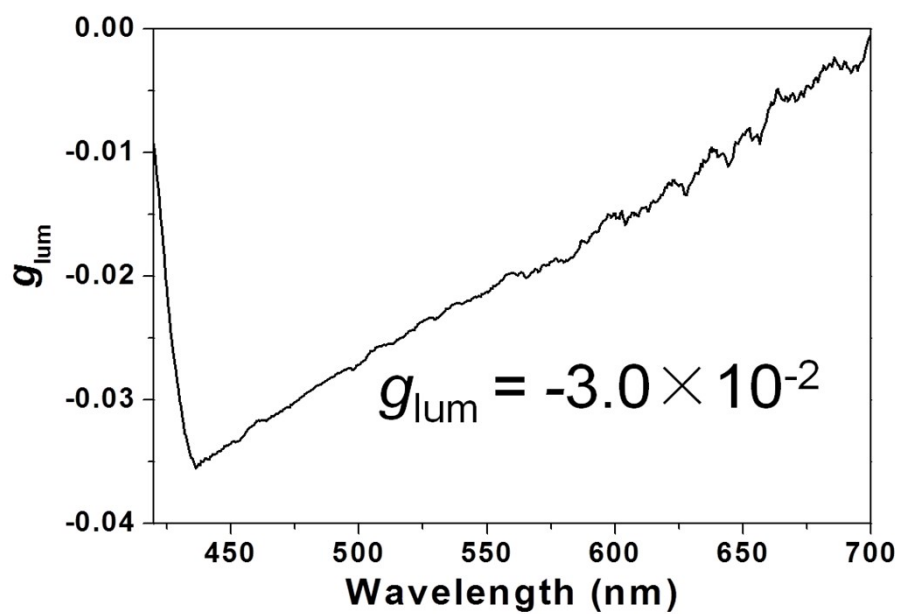


Fig. S11 CPL dissymmetry factor g_{lum} versus wavelength of Chol-CN-Py gel.

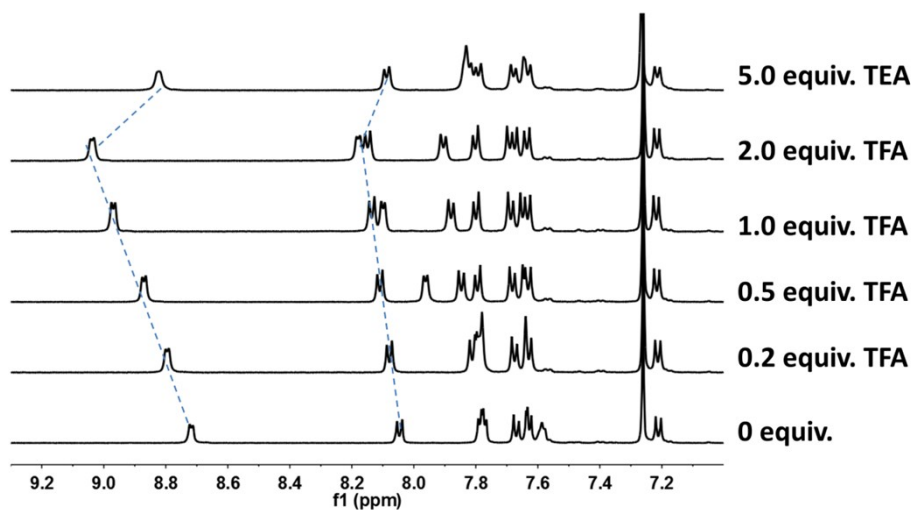


Fig. S12 1H NMR spectra of Chol-CN-Py in $CDCl_3$ (5 mM) upon the addition of 0-2 equivalent TFA and then 5 equivalent TEA.

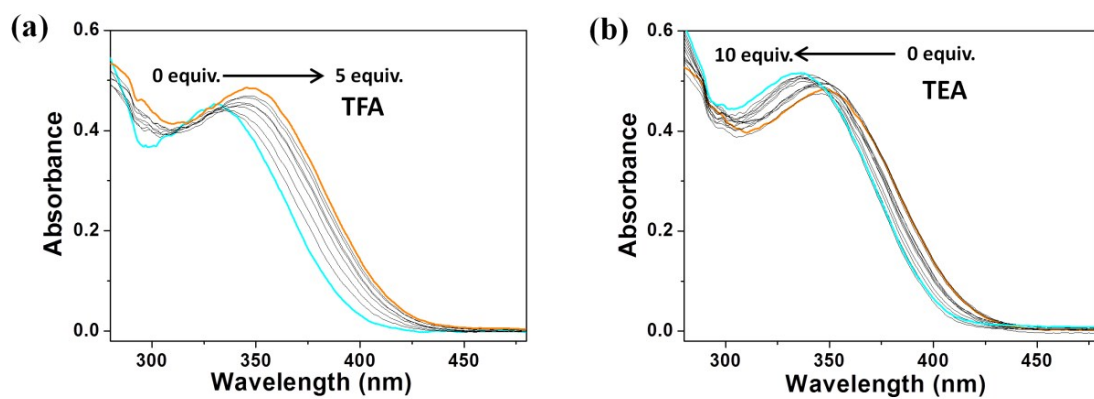


Fig. S13 (a) (b) UV-vis spectra of **Chol-CN-Py** (20 μM) under reversible TFA (0-5 equiv.) and TEA (0-10 equiv.) stimuli in DMF.

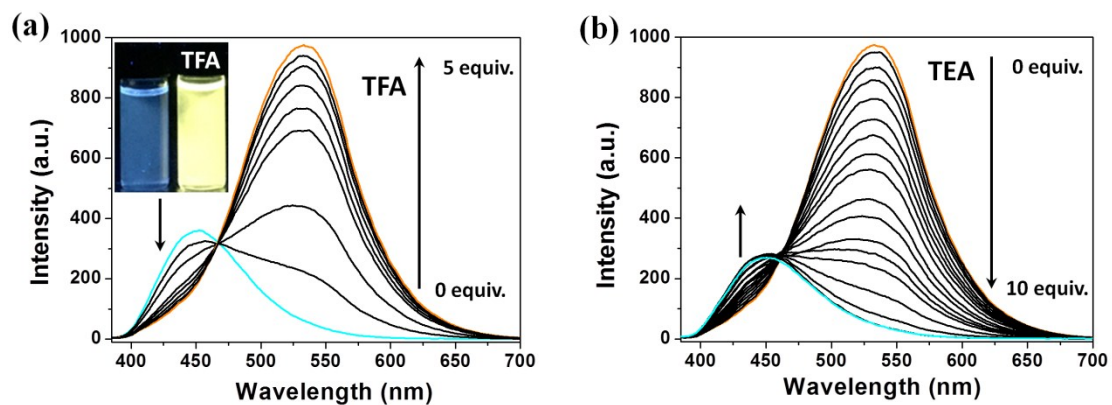


Fig. S14 (a) (b) Fluorescence spectra of **Chol-CN-Py** (20 μM , $\lambda_{\text{ex}} = 370 \text{ nm}$) under reversible TFA (0-5 equiv.) and TEA (0-10 equiv.) stimuli in DMF. Insets: photographs of the solution before (left) and after (right) TFA stimulus under illumination.

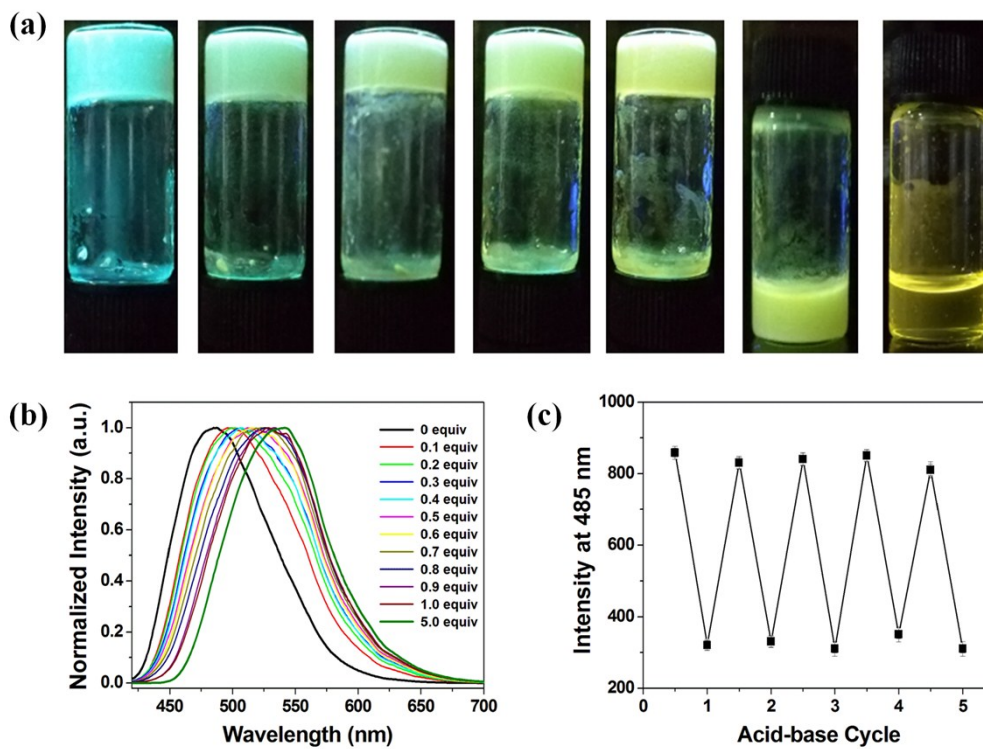


Fig. S15 (a) Photographs of gels containing different amounts of TFA under UV light (from left to right, the amount of TFA was 0.00, 0.20, 0.40, 0.60, 0.80, 1.00 and 5.00 equiv., respectively). (b) Normalized fluorescence spectra of gel with the addition of TFA ($\lambda_{\text{ex}} = 410 \text{ nm}$). (c) The reversible switch of emission intensity of the gel at 485 nm by alternating TFA and TEA stimuli.

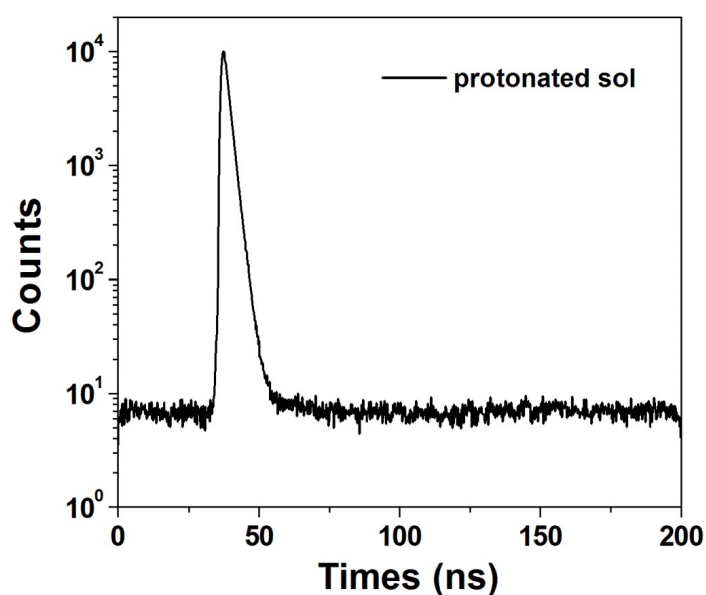


Fig. S16 Fluorescence kinetic profiles of the protonated sol.

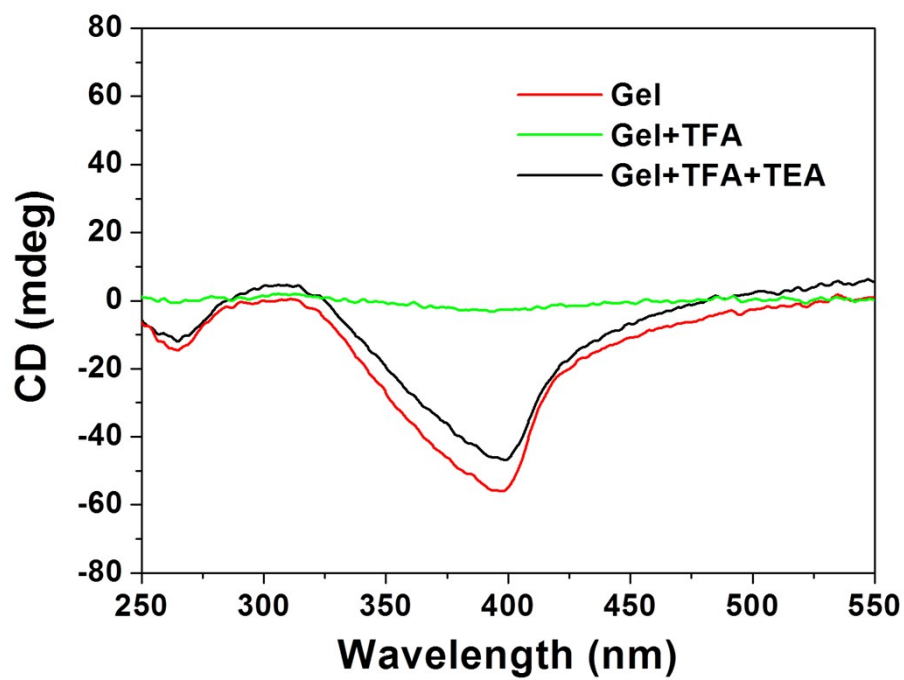


Fig. S17 CD spectra of Chol-CN-Py gel treated with TFA and TEA reversibly.

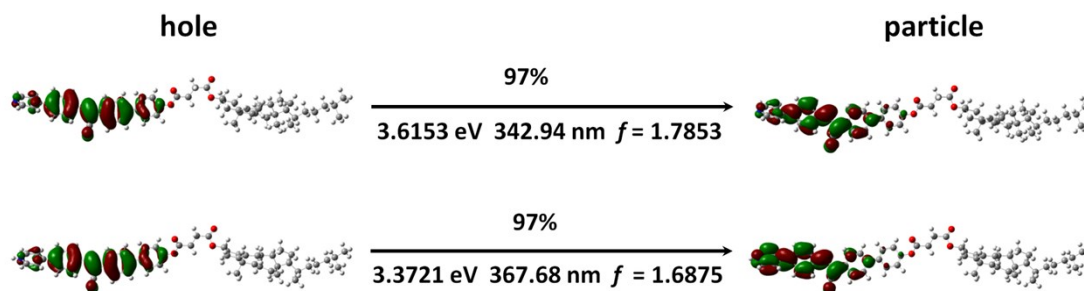


Fig. S18 NTOs from S_0 to S_1 of Chol-CN-Py (up) and protonated Chol-CN-Py (bottom) including energy levels, calculated absorption wavelength and oscillator strength (f).

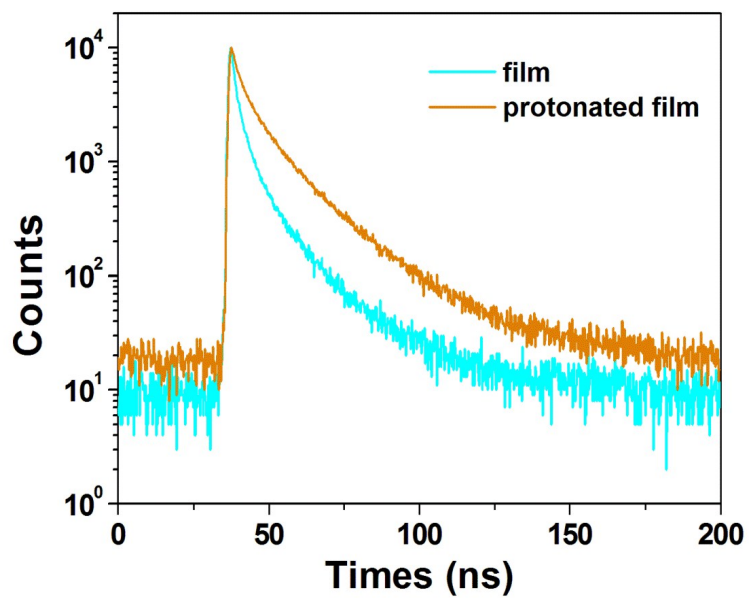


Fig. S19 Fluorescence kinetic profiles of the film and protonated film.

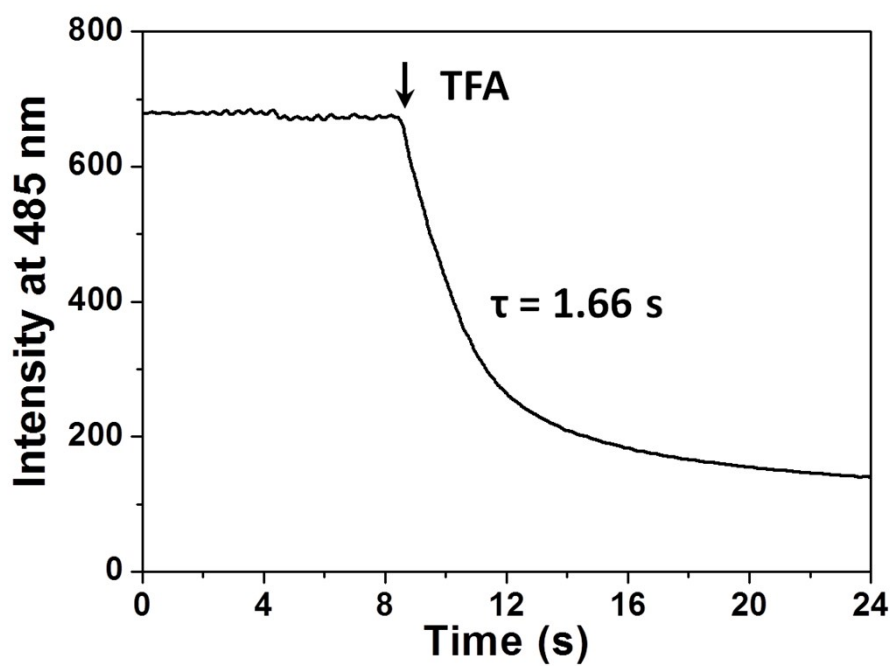


Fig. S20 Time-course of fluorescence quenching at 485 nm of the xerogel films upon exposure to saturated TFA.

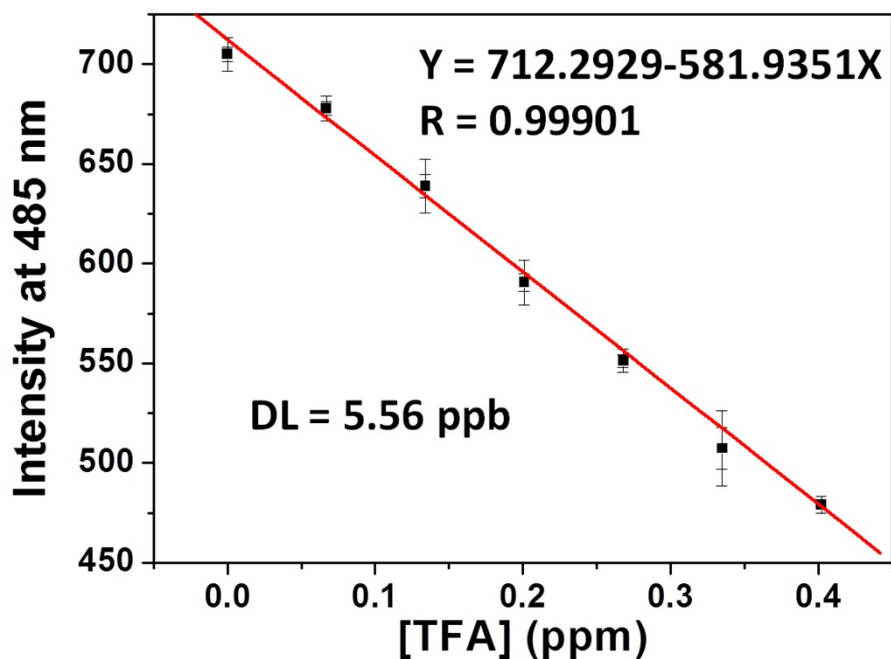


Fig. S21 The concentration-dependent fluorescence quenching efficiency of the films exposed to the TFA for 10 s. The limit of detection (DL) of **Chol-CN-Py** xerogel for TFA was calculated based on the fluorescence titration and determined from the following equation: $DL = 3\sigma/K$, where σ is the standard deviation of the blank solution; K is the slope of the calibration curve.

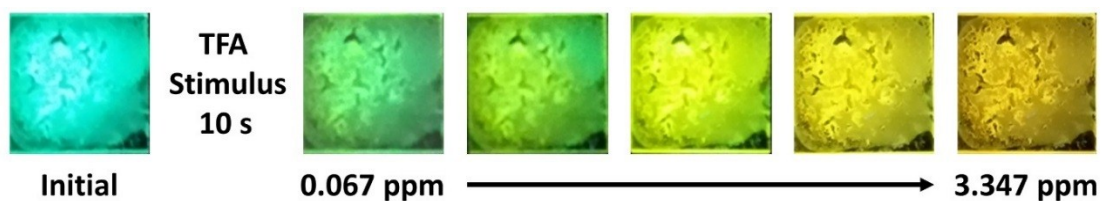


Fig. S22 The color transitions of xerogel films when exposed to TFA stimulus (0.067, 0.335, 1.340, 2.010, 3.347 ppm) for 10 s.

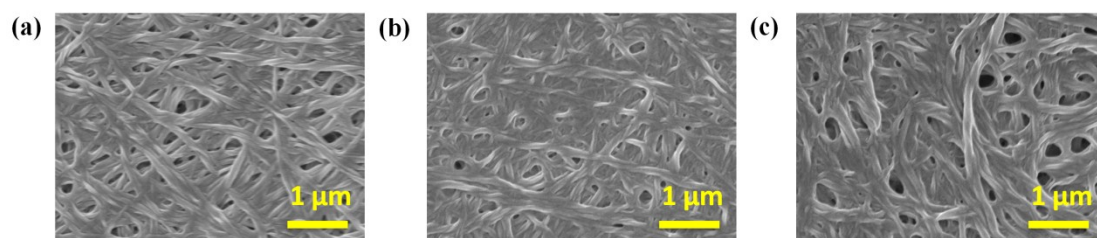


Fig. S23 SEM images of (a) xerogel film, (b) the one treated with 0.067 ppm TFA and (c) the one treated with 3.347 ppm TFA.